Main manuscript for

A widespread family of ribosomal peptide metallophores involved in bacterial adaptation to metal stress

Laura Leprevost[#1], Sophie Jünger[#2], Guy Lippens[3], Céline Guillaume[2], Giuseppe Sicoli[4], Lydie Oliveira[5], Alex Rivera-Millot[1&], Gabriel Billon[4], Céline Henry[5], Rudy Antoine[1], Séverine Zirah[2], Svetlana Dubiley[*3], Yanyan Li[*2], Françoise Jacob-Dubuisson[*1]

[1] Univ. Lille, U1018-UMR9017-CIIL-Center for infection and Immunity of Lille, F-59000 Lille, FRANCE

[2] Unit Molecules of Communication and Adaptation of Microorganisms (MCAM), UMR 7245 CNRS, MNHN, 75005 Paris, FRANCE

[3] Toulouse Biotechnology Institute, CNRS/INRAE/INSA/UPS, 31077 Toulouse, FRANCE

[4] Univ. Lille, CNRS, UMR 8516 - LASIRE, Laboratoire de Spectroscopie pour les Interactions, la Réactivité et l'Environnement F-59000 Lille, FRANCE

[5] INRAE-AgroParisTech-Univ. Paris-Saclay, MICALIS, 78352 Jouy-en Josas, FRANCE

[#] contributed equally

[&] current address: INRS-Centre Armand-Frappier Santé Biotechnologie, Bacterial Symbionts Evolution, Laval, Quebec H7V 1B7, Canada

[*] correspondence: svetlana.dubiley@gmail.com; yanyanli@mnhn.fr; francoise.jacob@ibl.cnrs.fr

Author contributions: GL, RA, SD, SZ, YL, FJD designed research; LL, SJ, GL, CG, GS, LO, ARM, GB, CH, RA, SD performed research; LL, SJ, GL, CG, GS, LO, ARM, GB, CH, RA, SZ, SD, YL, FJD analyzed data; LL, SJ, GL, SD, SZ, YL, FJD wrote the paper.

Competing interest statement: The authors declare no competing interests.

Classification: Biological Sciences - Biochemistry - Microbiology

Keywords: RiPP, metallophore, MNIO enzyme

This PDF file includes: Main text and Figures 1 to 5

This article was deposited as a preprint in BioRxiv (BIORXIV/2024/585515)

Abstract

Ribosomally synthesized and post-translationally modified peptides (RiPPs) are a structurally diverse group of natural products that bacteria employ in their survival strategies. Herein, we characterized the structure, the biosynthetic pathway and the mode of action of a new RiPP family called bufferins. With thousands of homologous biosynthetic gene clusters throughout the eubacterial phylogenetic tree, bufferins form by far the largest family of RiPPs modified by multinuclear non-heme iron-dependent oxidases (MNIO, DUF692 family). Using *Caulobacter vibrioides* bufferins as a model, we showed that the conserved Cys residues of their precursors are transformed into 5-thiooxazoles, further expanding the reaction range of MNIO enzymes. This rare modification is installed in conjunction with a partner protein of the DUF2063 family. Bufferin precursors are the first examples of bacterial RiPPs found to feature an N-terminal Sec signal peptide and thus to be exported by the ubiquitous Sec pathway, a new paradigm in the RiPP field. Other original features of bufferins are their large size and protein-like fold, which blurs the line between modified peptides and proteins. We reveal that bufferins are involved in copper homeostasis, and their metal-binding propensity requires the thiooxazole heterocycles. Bufferins enhance bacterial growth under copper stress by sequestering excess metal ions in the periplasm. Our study thus describes a large family of RiPP metallophores and unveils a widespread but overlooked metal homeostasis mechanism in eubacteria likely to be relevant to One-Health strategies.

Significance statement

Copper is both essential and toxic in excess. Bacteria face copper in their environments, notably in phagocytes, hence they have developed several defense mechanisms. We discovered a widespread strategy of protection from copper, through the biosynthesis of natural products that we call bufferins. Bufferins are ribosomally synthesized post-translationally modified peptides

(RiPPs), natural products with key roles in bacterial physiology and ecology. Bufferins enhance bacterial growth under copper stress by complexing with the metal using thiooxazole heterocycles that result from enzymatic modification of cysteine residues. With thousands of homologs throughout the eubacterial phylogenetic tree, bufferins represent a highly prevalent strategy of adaptation to metal stress. They are larger in size than most RiPPs, expanding the concept of RiPPs to modified proteins.

Main text

Introduction

Ribosomally synthesized and post-translationally modified peptides (RiPPs) are natural products with a tremendous variety of structures and biological activities (1-3). They are synthesized from a gene-encoded precursor peptide, generally composed of an N-terminal leader sequence and a core sequence where post-translational modifications (PTMs) occur. In many cases, a pathway-specific RiPP recognition element (RRE) domain interacts with the leader sequence and mediates recruitment of the modification enzymes (4-6). RRE domains are thus a hallmark of RiPP biosynthesis. The vast structural diversity of RiPPs is conferred by virtually unlimited possibilities of chemical transformations. An emerging family of PTM enzymes is the DUF692 family of multinuclear non-heme iron dependent oxidases (MNIOs) that catalyze various reactions in the biosynthesis of diverse RiPPs, mostly but not exclusively on Cys residues (7-13). These reactions include oxazolone coupled to thioamide formation, excision of cysteine β-methylene, Cys-involved macrocyclization, and C-C and C-N cleavages (7, 8, 11-13). However, the full spectrum of MNIO activities remains far from being fully appreciated.

Four-gene *gig* operons (*gig* for gold-induced genes) encoding DUF692-family proteins were identified in the genomes of several microbial species (*SI* Fig. S1). In *Cupriavidus*

85 *metallidurans*, *Legionella pneumophila*, and *Caulobacter vibrioides*, the expression of these
86 operons is induced under various transition metal stresses that include gold, cadmium, copper,
87 etc., whereas in *Bordetella pertussis* it is controlled by the master regulator of virulence BvgAS
88 (14-18). Orthologous operons were notably found in methane-oxidizing bacteria (19).
89 However, despite genetic evidence for an involvement in the copper-resistant phenotype in *C.*
90 *metallidurans* (20), the function of these operons remains elusive. Based on their composition,
91 we speculated that they are biosynthetic gene clusters (BGCs) whose products could represent
92 a new RiPP family. Unlike all previously described RiPPs however, these putative precursors
93 have Sec signal peptides. They are also markedly larger than known MNIO-modified RiPP
94 precursors. Using genetic, structural, and bioinformatic analyses, we questioned the function,
95 the mode of action, and the prevalence of *gig*-like operons in bacteria.

96 We report the characterization of the products of the *C. vibrioide*s *gig*-like BGCs, the first
97 representative of bufferins, a new family of RiPPs. We revealed that bufferins are small protein
98 metallophores containing a rare 5-thiooxazole modification of cysteine residues. The joint
99 action of the DUF692 (MNIO) and DUF2063 proteins is required to install this post-
100 translational modification, which is new to the MNIO family of enzymes. We showed that the
101 *C. vibrioides* bufferins protect bacteria against toxic concentrations of copper by sequestering
102 the excess metal in the periplasm. Our bioinformatic study suggests that bufferins represent an
103 overlooked transition metal defense mechanism very common in Hydrobacteria and
104 Terrabacteria.

105

106 ## Results

107 ***Large new RiPP family involving MNIOs.*** We performed an *in-silico* analysis of the
108 CCNA_03363-03366 operon of *C. vibrioides*, hereafter named *buf1*, to gain insight into gene
109 functions. CCNA_03363 encodes a DUF2282-family protein (BufA1), whose members are 80-

110 120 residues long and harbor four Cys residues (Cys^{I} to Cys^{IV}) and a predicted Sec signal
111 peptide (Fig. 1A). We hypothesized that BufA1 is an unusually long precursor peptide whose
112 translocation across the cytoplasmic membrane would rely on the ubiquitous Sec export
113 pathway rather than on a specialized export system as is often the case for secreted RiPPs (21).
114 The AlphaFold2 model predicts that the 68-residue long BufA1 core peptide contains a 2-
115 stranded β sheet and some α-helical structure (*SI* Fig. S1). It thus folds into a small protein
116 rather than being a totally unstructured peptide.

117 The product of CCNA_03364 (BufB1) belongs to the MNIO family, whereas
118 CCNA_03365 codes for a protein (BufC1) with an uncharacterized N-terminal DUF2063
119 domain. The predicted structural model of BufC1 revealed that its C-terminal domain is related
120 to RRE domains (4-6) (*SI* Fig. S1). In light of recent discoveries of MNIOs involved in RiPP
121 biosynthesis (7-13), we hypothesized that BufB1 and BufC1 would install modifications on Cys
122 residues of BufA1. Finally, CCNA_03366 encodes a putative DoxX-type oxido-reductase,
123 BufD1 (22, 23).

124 Inspection of the *C. vibrioides* genome identified a second operon, the *buf2* BGC
125 (CCNA_02999-03001) (Fig. 1A) which encodes homologs of BufB1 (CCNA_03000) and
126 BufC1 (CCNA_02999) but lacks a *bufD1*-like gene. Like BufA1, its putative precursor peptide
127 BufA2 (CCNA_03001) possesses a Sec signal peptide. Its 61-residue core peptide contains six
128 Cys residues (Cys^{I} to Cys^{VI}) (Fig. 1A). Although its predicted 3D structure is very similar to
129 that of BufA1, this small protein does not have a corresponding profile in the databases of
130 protein families (*SI* Fig. S1).

131 To evaluate the abundance of homologous BGCs, we collected >14,000 MNIO protein
132 sequences from the NCBI non-redundant database. The retrieved sequences are widely
133 distributed throughout Pseudomonadota, Terrabacteria, Myxococcota,
134 Fibrobacteres/Chlorobi/Bacterioidetes, Planctomycetes/Verrucomicrobia/Chlamydia, and

135 Acidobacteriota. We analyzed their genomic contexts and collected associated genes coding for
136 putative bufferin-like precursors, i.e., small proteins with Cys residues and a predicted Sec
137 signal peptide. Thousands of these were collected, some of which are markedly larger than
138 typical RiPP precursors and harbor numerous Cys residues (detailed *in silico* analyses will be
139 published separately). In a sequence similarity network (SSN) constructed with these proteins,
140 the largest cluster corresponds to the DUF2282 signature, including *C. vibrioides* BufA1 (Fig.
141 1B). BufA2 of *C. vibrioides* belongs to the second largest cluster of proteins characterized by
142 six or twelve conserved Cys residues, which we named BUF_6/12Cys (Fig. 1B,C). Of note,
143 BUF_6/12Cys proteins were previously identified in Antarctic soil metagenomes (24). Parallel
144 SSN analyses of the MNIO superfamily (Fig. 1D) showed that those coded in the DUF2282
145 and BUF_6/12Cys BGCs belong to the most populated sequence cluster, distinct from small
146 clusters of MNIOs involved in the biosynthesis of other RiPP types (7, 9-11, 13). Together our
147 data indicate that bufferins currently form the largest group of MNIO-associated RiPPs.
148
149 ***Bufferins mediate adaptation to copper stress***. In *C. vibrioides*, *buf1* and *buf2* BGCs belong to
150 the SigF-controlled, core regulon of copper stress (15, 17, 25). To test if they could be up-
151 regulated by other biologically relevant metals, we generated reporter fusions within *bufA1* and
152 *bufA2* and confirmed that both are induced by high concentrations of Cu^{2+}, but not by Fe^{2+}, Zn^{2+}
153 or Mn^{2+} (Fig. 2A; *SI* Fig. S2).
154 To determine if bufferins, the putative RiPP products of the *buf* BGCs, contribute to
155 adaptation to copper stress, we prepared *C. vibrioides* deletion mutants that express a single
156 (Cv_{buf1} and Cv_{buf2}) or neither BGC (Cv_{DKO}). Cv_{DKO} grew more slowly than the parental Cv_{WT}
157 strain when $CuSO_4$ was added to the growth medium, unlike Cv_{buf1} or Cv_{buf2} (Fig. 2B). Thus,
158 bufferins enhance growth under copper stress and are functionally redundant. To confirm that
159 a single BGC is sufficient to protect bacteria from excess copper, we performed a gain-of-

160 function experiment. Expression of *buf1ABCD* in an *Escherichia coli* laboratory strain
161 enhanced survival of bacteria exposed to a bactericidal concentration of $CuSO_4$ (Fig. 2C).
162 We then asked whether the bufferins would confer an advantage on *C. vibrioides* in biotic
163 interactions. Since amoeba notably use copper against their bacterial preys (26), a predation
164 assay was performed. We attempted to measure survival of *C. vibrioides* after ingestion by
165 *Dictyostelium discoidum*, a well-established mode organism for the study of phagocytosis.
166 However, as these assays were unsuccessful, we tested if the presence of the *buf* BGCs might
167 slow down bacterial killing. We placed amoebal suspensions onto bacterial lawns, and after
168 incubation we determined bacterial densities in the contact zones by densitometry scanning.
169 Larger zones of bacterial clearance were observed for the Cc_{DKO} than for the Cc_{WT} strain,
170 consistent with a protective role of bufferins in this context (Fig. 2D).
171
172 ***Characterization of bufferin PTMs***. To identify the PTMs of bufferins, we engineered an
173 IPTG-inducible version of SigF to control expression of their BGCs in *C. vibrioides*. The
174 metabolic profiles of IPTG-treated Cv_{buf1}(pSigF) and Cv_{buf2}(pSigF) were analyzed by liquid
175 chromatography coupled to mass spectrometry (LC-MS) and compared to that of Cv_{DKO}(pSigF)
176 to reveal peptide species only present in the *buf*-expressing strains. In Cv_{buf1}(pSigF), a major
177 species exhibited a mass matching that of BufA1 with the Sec signal peptide cleaved off and a
178 -10 Da mass shift (Fig. 3A; *SI* Fig. S3 and Table S1), suggesting that the core peptide
179 accumulates in the periplasm and contains post-translational modifications of one or more
180 residues. A second form with a -12 Da mass shift was also detected, but not systematically, and
181 it disappeared upon freeze-thawing of cell extracts. The most stable product with a -10 Da mass
182 shift is considered the mature peptide product and was named bufferin 1 (Buf1). Similarly,
183 Cv_{buf2}(pSigF) produced a major peptide product with a -18 Da mass shift, called bufferin 2
184 (Buf2), and a minor species with a -20 Da mass shift (*SI* Fig. S3 and Table S1).

185 To test the hypothesis that mature bufferins contain modified Cys residues and disulfide
186 (S-S) bonds, we performed reduction and alkylation treatment of the peptides. This yielded
187 species carrying three or four alkylated groups for Buf1 and four, five or six alkylated groups
188 for Buf2 (*SI* Fig. S4), suggesting that the expected PTMs do not affect Cys residues or result in
189 alkylation-sensitive groups. MS analyses of trypsin-digested, alkylated bufferins revealed that
190 Cys^{I} (Cys12) and Cys^{IV} (Cys52) in Buf1 (numbering according to the core peptide, see Fig. 1)
191 had mass increments corresponding to alkylation only, indicative of unmodified residues (*SI*
192 Fig. S5). By contrast, in the central tryptic peptide containing Cys^{II} (Cys23) and Cys^{III} (Cys31),
193 both Cys residues carry mass increments corresponding to alkylation with additional -4.03 Da
194 mass shifts (Fig. 3B), as proposed by the untargeted PTM search solution SpecGlobX (27).
195 To confirm that Cys residues are required for Buf1 function, we constructed strains with
196 the conserved Cys residues replaced with Ser, separately or in combinations. Consistent with
197 the proposed modifications of Cys^{II} or Cys^{III}, the substitution of either of them yielded peptides
198 with mass shifts of -6 Da relative to the calculated mass of the mutated peptide (*SI* Fig. S6). We
199 tested the ability of the mutated BufA1 to protect *C. vibrioides* from excess copper. All mutant
200 strains grew more slowly than the parental Cv_{buf1} in the presence of $CuSO_4$ (*SI* Fig. S7),
201 indicating the importance of modified and unmodified Cys residues for function. Altogether,
202 the data are consistent with the presence of an S-S bond between Cys^{I} and Cys^{IV} and Cys^{II} and
203 Cys^{III} being targets of 4-electron oxidation reactions that generate alkylation-sensitive groups.
204 The Buf1 congener product with a -12 Da mass shift would correspond to a form with a labile
205 S-S bond between the modified residues. Similarly, in Buf2, in addition to the unmodified Cys^{I}
206 (Cys24) and Cys^{VI} (Cys50) likely forming an S-S bond (*SI* Fig. S1), the central Cys residues
207 carry -4.03 Da shifts (*SI* Fig. S8).
208 To facilitate bufferin purification and characterization, we added C-terminal tags to BufA1
209 (*SI* Table S1). The affinity-purified tagged Buf1 was fully modified (*SI* Fig. S9). To probe if

210 the modified Cys residues may be part of heterocycles as in other MNIO-modified RiPPs (7,
211 10), we recorded UV-visible absorption spectra of Buf1 and the Buf1$^{CysIISer+CysIIISer}$ variant.
212 Consistent with the presence of aromatic heterocycles (28), the spectrum of the former showed
213 a broad absorbance peak extending to 310 nm, unlike that of the latter (Fig. 3C). The spectrum
214 of recombinant Buf2 showed a similar absorbance maximum around 305 nm (*SI* Fig. S10).
215
216 ***PTM identification by NMR***. To increase the yield of bufferin for structural elucidation by
217 NMR, we co-expressed *bufA1* encoding an N-terminal His_6-SUMO-tag with *bufB1* and *bufC1*
218 in *E. coli*. Purification of modified BufA1 followed by trypsin digestion and preparative HPLC
219 allowed the preparation of the Cys^{II}- and Cys^{III}-containing 19-mer peptide at a milligram scale
220 (*SI* Fig. S11). Its ^{1}H spectrum indicated two groups of anomalous resonances (*SI* Fig. S12). By
221 combining homonuclear ROESY and TOCSY experiments (29), they were assigned to the
222 amide protons of Lys24 and Ala32 that follow the modified Cys^{II} and Cys^{III} residues,
223 respectively, and to the Hα protons of Asp22 and Ser30 that precede them (Fig. 3D). Further
224 analysis of these spectra showed the absence of both Hα and NH protons for the modified Cys
225 residues. The absence of the latter was verified on a natural abundance ^{1}H, ^{15}N HSQC spectrum
226 (*SI* Fig. S12). These data suggest that their N and Cα atoms are part of heterocycles.
227 A ^{1}H, ^{13}C HSQC experiment showed correlations from the Asp22 and Ser30 Hα atoms to
228 their own Cα carbons at 48.1 and 52.4 ppm, respectively, 6 ppm higher than their random coil
229 values (30). The ^{1}H, ^{13}C HMBC spectrum connected the same Hα protons to carbon atoms at
230 161.1 and 159.8 ppm, respectively (*SI* Fig. S12). We produced a uniformly ^{13}C,^{15}N-labeled
231 modified BufA1 molecule in *E. coli* and used its central tryptic peptide to obtain further carbon
232 assignments on the basis of triple-resonance NMR experiments (31, 32). In the HNCACB
233 experiment, we found no resonances that could correspond to upstream neighbors for Lys24 or
234 Ala32, confirming that the Cα carbons of modified Cys^{II} and Cys^{III} do not resonate at the typical

235 50-ppm value expected for Cys residues (Fig. 3E). In a HNCO experiment starting from the
236 amide groups of Lys24 or Ala32, we found values around 184 ppm for the C=O carbon atoms
237 of both modified Cys residues (Fig. 3F), far from 175-ppm and 200-ppm values expected for
238 such atoms in random-coil and thio-amide peptides, respectively (30, 33). By increasing the
239 resolution and varying the offset of the decoupling pulse during the C=O evolution period, we
240 determined a 90-Hz coupling constant of both carbonyls with carbon atoms whose chemical
241 shift is ~120 ppm, consistent with their absence in the HNCACB experiment (Fig. 3G). Both
242 parameters point to the C=O carbon atoms of the modified Cys residues connected to carbon
243 atoms in aromatic rings (34).

244 Comparisons of the chemical shifts assigned on the modified BufA1 peptide with those
245 found for a 5-thiooxazole-containing peptide (28) show the same 6-ppm upfield shift of the Cα
246 carbon of the preceding residue, the presence of similar carbon resonances at 120 and 160 ppm,
247 and the 90-Hz coupling constant of the following carbonyl towards an aromatic ring carbon.
248 Together with the MS data and the characteristic spectrophotometric spectrum (28), we
249 conclude that the Buf1 modification implies cyclization of its central Cys residues to form
250 thiooxazole groups (Fig. 3H).

251

252 ***Copper binding by bufferin 1.*** Since heterocycles can be involved in copper binding (35), we
253 interrogated if bufferins can complex with copper, which could be the basis for their protective
254 effect. As attempts to saturate Buf1 with copper *in vitro* were inefficient (*SI* Fig. S13), we
255 investigated complex formation *in vivo* by treating cultures of *bufABCD1*-expressing *E. coli*
256 with $CuSO_4$ for three hours prior to bufferin purification. Native MS analysis showed that
257 purified Buf1 thus produced was fully loaded with copper (Fig. 4A). Pulsed electron
258 paramagnetic resonance (EPR) spectra confirmed that Buf1 binds paramagnetic Cu^{2+}, and
259 spectral simulations indicated coordinating N atom(s) (36) (Fig. 4B; *SI* Tables S2 and S3).

260 To gain further insight into the binding site, we produced a $^{15}N,^{13}C$-labeled Buf1 sample
261 and recorded triple resonance spectra to assign its resonances. Simultaneously, we used the ^{1}H,
262 ^{15}N HSQC plane as a basis for HSQC-NOESY and TOCSY experiments to confirm the
263 assignments and gain some knowledge on structural aspects of Buf1. The sequential assignment
264 was interrupted by the modified Cys residues, as expected. Interestingly, amide resonances of
265 the tryptic peptide and of the same segment in the full-length bufferin do not correspond at all,
266 suggesting that the full-length sequence imposes structural constraints on the thiooxazole-
267 containing loop. Part of these likely come from the β sheet spanning two short strands in the
268 structural model, Thr9-Tyr13 and Trp44-Lys48 (*SI* Fig. S1), that we confirmed experimentally
269 through the strong Hα(i-1) – HN(i) NOE contacts between residues in these segments and the
270 cross-strand NOE contacts between the amide protons of Lys45 and Cys12, and of Val47 and
271 Glu10, respectively (*SI* Fig. S14). PTMs of the Cys residues hence do not interfere with the 3D
272 structure predicted for the unmodified sequence.
273 A comparison of the spectra of the bufferin produced with or without copper showed many
274 peaks unchanged, some experiencing a shift and a signal reduction, and yet others disappearing
275 altogether (Fig. 4C). The latter most probably concern residues close to the paramagnetic Cu^{2+}
276 ion. In particular, disappearance of the peaks corresponding to direct neighbors of the
277 heterocycles, such as Lys24, Ser30 and Ala32, confirms that the thiooxazoles are involved in
278 Cu^{2+} coordination. Interestingly, signals of Thr9, Trp44, Met46 and Lys48 predicted on the β-
279 sheet face oriented towards the thiooxazole-containing loop also disappeared. Our data thus
280 support that the thiooxazole cycles and residues of the β sheet are involved in copper binding.
281
282 ***BufB1 and BufC1 are required for post-translational modification of bufferin.*** To dissect the
283 role of individual *buf* genes, we constructed Cv_{buf1} derivatives that lack one or several genes
284 and tested their growth phenotypes in the presence of $CuSO_4$. All deletion strains except for

285 that lacking *bufD1* displayed slow-growth phenotypes, showing that BufA1, BufB1 and BufC1,
286 but not BufD1, are required for the function (Fig. 5A).

287 Since MNIO enzymes require Fe^{II} and Fe^{III} ions for activity (9, 12), purified BufB1 was
288 analyzed by inductively coupled plasma - optical emission spectrometry, showing the presence
289 of two Fe ions. To reveal the role of BufB1 and BufC1 in the bufferin maturation, we
290 reconstituted the modification reaction *in vitro* using the purified proteins (*SI* Fig. S15). LC-
291 MS analyses showed that BufA1 was converted to a species with a -8 Da mass shift only when
292 BufB1 and BufC1 were present (Fig. 5B). Trypsin digestion of the *in vitro* modified BufA1
293 yielded the 19-residue peptide harboring the thiooxazole groups as confirmed by MS/MS
294 analyses (Fig. 5C). Together with the gene inactivation data, these experiments established that
295 BufB1 and BufC1 are required and sufficient to install the PTMs on BufA1.

296

297 ***The signal-peptide sequence is dispensable for heterocycle formation***. A notable feature of
298 bufferin biosynthesis is that the precursor peptide harbors a Sec signal peptide, which is
299 unprecedented in bacterial RiPPs precursors. We investigated if this sequence also acts as a
300 leader peptide required for Cys transformation. Using the SUMO-*bufA1/bufB1/bufC1 E. coli*
301 co-expression system, the *bufA1* gene was mutated to generate variant precursors with the signal
302 peptide truncated eight residues from the N-terminus (BufA1(-8 aa)) or completely removed
303 (BufA1(CP)). Subsequent LC-MS analysis of purified BufA1 after SUMO-tag cleavage
304 indicated that both truncated precursors were still modified with a -10 Da shift, consistent with
305 the presence of two thiooxazoles and one S-S bond (Fig. 5D). Thus, the signal peptide is
306 dispensable for the installation of the PTMs, suggesting that main recognition determinants of
307 the precursor peptide by the BufB1C1 machinery are located within the core sequence.

308

309

310 ## Discussion

311 Here we report a widespread bacterial strategy for metal homeostasis based on the synthesis of
312 periplasmic RiPP metallophores. Incidentally, we also solved the conundrum of the gold-
313 induced genes found in environmental and pathogenic bacteria (14-16). Bufferins form a new
314 RiPP family with original features and a new function. We showed that they harbor a rare
315 modification, 5-thiooxazole, installed by an MNIO enzyme. With thousands of homologs,
316 bufferins are highly prevalent in eubacteria and represent the largest family of MNIO-modified
317 RiPPs.

318 The biosynthesis of bufferins involves unique features. To our knowledge they are the first
319 RiPPs naturally exploiting Sec signals for efficient translocation to the periplasm. Peptides with
320 bulky modifications or macrocycles would be poor substrates of the Sec machinery due to the
321 pore size of SecY (37). Although bufferins harbor an S-S bond formed macrocycle, the latter is
322 most likely installed in the oxidizing periplasmic environment after export. The use of
323 'generalist' systems, Sec and signal-peptidase, for export and proteolytic maturation is a new
324 paradigm in the RiPP field.

325 The precursors and mature forms of bufferins are large compared to those of other MNIO-
326 modified RiPPs, and our *in-silico* analyses identified yet larger bufferin-like precursors of more
327 than 200 residues with numerous Cys residues. Thus, the bufferin family appears to harbor a
328 continuum from modified peptides to proteins, which expands the concept of *bona fide* RiPPs
329 to what could be 'RiPProteins'.

330 The conversion of Cys to 5-thiooxazole represents a new reaction catalyzed by MNIOs,
331 further highlighting their chemical versatility. Intense efforts have been made recently to
332 explore the chemical space of RiPPs undergoing MNIO-catalyzed transformations (7, 8, 11, 13,
333 38). In line with previous work on Cys-modifying MNIO enzymes, BufB would similarly make

334 use of the mixed-valent iron center and proceed by an intermediate step of proton abstraction
335 from the Cβ of cysteine (9, 10, 12, 13) (SI Fig. S16).

336 We demonstrated that model bufferins are involved in copper homeostasis by complexing
337 with the metal in the periplasm. This novel function for RiPPs contrasts with that of other
338 MNIO-modified metallophores, methanobactins, a phylogenetically restricted family of RiPPs
339 which essentially scavenge copper ions in the extracellular milieu for its provision to
340 cuproprotein clients (39-42). The mode of binding of bufferins also differs from that of
341 methanobactins. Notably, *in vivo* formation of the bufferin-Cu^{2+} complex most likely occurs
342 while the unfolded bufferin emerges from the Sec machinery in the periplasm and folds around
343 copper, which explains that our *in vitro* loading attempts were not successful. The defensive
344 role of bufferins is reminiscent of those of non-ribosomal peptides, anthrochelin and
345 yersiniabactin (43, 44), although the putative multiple metal binding sites of large bufferins
346 suggest that some of them might serve as intracellular metal reservoirs. Future studies on this
347 large, diverse family will likely also unveil roles for bufferins in the homeostasis of other
348 transition metals.

349 Copper is a major metal pollutant from anthropic sources (45, 46), and bufferins represent
350 a previously unknown but highly prevalent mechanism of bacterial adaptation likely relevant
351 in the environment, agriculture and healthcare. In *C. vibrioides*, their expression is induced at
352 high copper concentrations, suggesting that they come into play after other defense systems are
353 overwhelmed. Genetic determinants that provide environmental species with protection against
354 transition metals can contribute to the emergence of opportunistic pathogens (47), as
355 exemplified by *Legionella pneumophila* which harbors up to six bufferin BGCs. Bufferins are
356 most likely beneficial to bacteria in host-pathogen interactions notably in phagosomal
357 compartments, which might account for their presence in *Bordetella pertussis, Neisseria*
358 *gonorrheae, Haemophilus influenzae* and *Pseudomonas aeruginosa* (26, 48, 49). From a more

359 applied perspective, it should be possible in the long term to engineer bufferin variants for
360 bioremediation purposes (3).

361

362 **Materials and methods**

363 ***Genetic constructs and growth conditions.*** Construction details, plasmids, recombinant strains,
364 primers and synthetic genes are described in *SI* Text and Tables S4 to S6, respectively.

365 ***Functional experiments.*** *C. vibrioides* growth curves were recorded using a TECAN Spark
366 plate reader, with OD_{600} measurements every 20 min. The gain-of-function experiment was
367 performed in *E. coli* expressing the *buf*1 operon under the control of an IPTG-inducible
368 promoter. The bacteria were challenged with 0.3 mM $CuSO_4$ for 4 hours. For the predation
369 experiments, *Dictyostelium discoidum* was placed in the center of bacterial lawns before
370 incubation at 20˚C for three days, and the densities of bacteria in the contact zones were
371 determined with ImageJ. Experimental details are in *SI* Text.

372 ***Bufferin production and purification***. For Buf1 or Buf2 production in *C. vibrioides*, strains
373 harboring the pSigF plasmid were grown overnight in PYE medium containing 100 μM IPTG,
374 and the bufferins were purified on Streptactin or Ni-NTA columns using standard procedures.
375 Production of isotopically labeled Buf1 was performed in *E. coli* BL21. For the *in vitro* assays,
376 N-His_6-SUMO-BufA1, N-His_6-BufB1 and N-His_6-BufC1 were produced in BL21(DE3),
377 purified on Ni-NTA columns, with 10 mM Tris(2-carboxyethyl)phosphine hydrochloride added
378 to all buffers for BufA1. Production of the trypsic peptide for NMR studies was performed in
379 BL21(DE3) co-expressing Sumo-BufA1, BufB1 and BufC1. The iron content of His_6-BufB1
380 was measured using an inductively coupled plasma - optical emission spectrometer (ICP-OES
381 5110 VDV, Agilent Technologies). Experimental details are provided in *SI* Text.

382 ***Peptide analyses by MS.*** All experimental details are given as *SI* text.

383 ***NMR analyses.*** The central tryptic peptide was purified by preparative HPLC. All NMR spectra
384 were recorded at 293 K on an 800-MHz NEO Bruker spectrometer equipped with a QCP
385 cryogenic probe head. Experimental details are in *SI* Text.

386 ***EPR experiments.*** Pulsed EPR experiments were performed on the Buf1^{twstr}-copper complex
387 using an ELEXSYS E-580 spectrometer (Bruker). Experimental details are in *SI* Text.
388 Numerical simulation of the spectra was conducted using the Matlab toolbox Easyspin 5.2.35.

389 ***Spectrophotometric copper binding assay***. This was performed as described (50).

390 ***Enzymatic assays in vitro***. Purified His-SUMO-BufA1 was digested with SUMO protease
391 before adding either or both N-His$_6$-BufB1 and N-His$_6$-BufC1. After incubation the mixtures
392 were analyzed by LC-MSMS. Details are presented as *SI* Text.

393 ***In silico analyses.*** The search for putative bufferin precursors and the SSN analyses are detailed
394 in *SI* Text.

395

396 **Acknowledgments.** We thank E. Lesne and G. Roy for initiating this work long ago, J.-M.
397 Saliou for preliminary MS analyses and J.-Y. Matroule and P. Cherry for providing *C.*
398 *vibrioides* strains, plasmids and protocols. This project was funded by the ANR grant CuRiPP
399 (ANR-22-CE44-0001-02) to FJD. L. Leprevost and S. Jünger were supported by PhD
400 fellowships of Lille University and the French Ministry of Education (ED 227 MNHN-SU),
401 respectively. S. Dubiley was supported as a Visiting Scientist by a fellowship of the Collège de
402 France. We thank the NMR facility of MetaToul (www.metatoul.fr). Metatoul is part of the
403 French National Infrastructure for Metabolomics and Fluxomics MetaboHUB-AR-11-INBS-
404 0010 (www.metabohub.fr), and is supported by the Région Midi-Pyrénées, the ERDF, the
405 SICOVAL and the French Minister of Education & Research, who are all gratefully
406 acknowledged. The LC-MS data were acquired at the MNHN bioorganic mass spectrometry
407 platform and the PAPPSO platform (http://pappso.inra.fr/en). For the EPR experiments the

408 financial support from the IR INFRANALYTICS FR2054 is acknowledged. ICP-OES
409 measurements were performed by V. Alaimo on the Chevreul Institute Platform (U-Lille /
410 CNRS). The Region Hauts de France and the French government are acknowledged for funding
411 this apparatus.

412

413 **References**

414 1. P. G. Arnison *et al.*, Ribosomally synthesized and post-translationally modified peptide natural
415 products: overview and recommendations for a universal nomenclature. *Nat Prod Rep* **30**, 108-160
416 (2013).

417 2. Y. Li, S. Rebuffat, The manifold roles of microbial ribosomal peptide-based natural products in
418 physiology and ecology. *J Biol Chem* **295**, 34-54 (2020).

419 3. M. Montalban-Lopez *et al.*, New developments in RiPP discovery, enzymology and engineering.
420 *Nat Prod Rep* **38**, 130-239 (2021).

421 4. B. J. Burkhart, G. A. Hudson, K. L. Dunbar, D. A. Mitchell, A prevalent peptide-binding domain
422 guides ribosomal natural product biosynthesis. *Nat Chem Biol* **11**, 564-570 (2015).

423 5. J. R. Chekan, C. Ongpipattanakul, S. K. Nair, Steric complementarity directs sequence promiscuous
424 leader binding in RiPP biosynthesis. *Proc Natl Acad Sci U S A* **116**, 24049-24055 (2019).

425 6. A. M. Kloosterman, K. E. Shelton, G. P. van Wezel, M. H. Medema, D. A. Mitchell, RRE-Finder:
426 a Genome-Mining Tool for Class-Independent RiPP Discovery. *mSystems* **5** (2020).

427 7. R. S. Ayikpoe, L. Zhu, J. Y. Chen, C. P. Ting, W. A. van der Donk, Macrocyclization and Backbone
428 Rearrangement During RiPP Biosynthesis by a SAM-Dependent Domain-of-Unknown-Function
429 692. *ACS Cent Sci* **9**, 1008-1018 (2023).

430 8. V. T. Chioti, K. A. Clark, J. G. Ganley, E. J. Han, M. R. Seyedsayamdost, N-Calpha Bond Cleavage
431 Catalyzed by a Multinuclear Iron Oxygenase from a Divergent Methanobactin-like RiPP Gene
432 Cluster. *J Am Chem Soc* 10.1021/jacs.3c11740 (2024).

433 9. C. Dou *et al.*, Crystal structure and catalytic mechanism of the MbnBC holoenzyme required for
434 methanobactin biosynthesis. *Cell Res* **32**, 302-314 (2022).

435 10. G. E. Kenney *et al.*, The biosynthesis of methanobactin. *Science* **359**, 1411-1416 (2018).

436 11. D. T. Nguyen *et al.*, Biosynthesis of macrocyclic peptides with C-terminal beta-amino-alpha-keto
437 acid groups by three different metalloenzymes. *Acs Central Science* 10.1021/acscentralsci.4c00088
438 (2024).

439 12. Y. J. Park *et al.*, A mixed-valent Fe(II)Fe(III) species converts cysteine to an oxazolone/thioamide
440 pair in methanobactin biosynthesis. *Proc Natl Acad Sci U S A* **119**, e2123566119 (2022).

441 13. C. P. Ting *et al.*, Use of a scaffold peptide in the biosynthesis of amino acid-derived natural products.
442 *Science* **365**, 280-284 (2019).

443 14. K. Jwanoswki *et al.*, The Legionella pneumophila GIG operon responds to gold and copper in
444 planktonic and biofilm cultures. *PLoS One* **12**, e0174245 (2017).

445 15. C. Kohler, R. F. Lourenco, G. M. Avelar, S. L. Gomes, Extracytoplasmic function (ECF) sigma
446 factor sigmaF is involved in Caulobacter crescentus response to heavy metal stress. *BMC Microbiol*
447 **12**, 210 (2012).

448 16. N. Wiesemann *et al.*, Influence of copper resistance determinants on gold transformation by
449 Cupriavidus metallidurans strain CH34. *J Bacteriol* **195**, 2298-2308 (2013).

450 17. L. Maertens, P. Cherry, F. Tilquin, R. Van Houdt, J. Y. Matroule, Environmental Conditions
451 Modulate the Transcriptomic Response of Both Caulobacter crescentus Morphotypes to Cu Stress.
452 *Microorganisms* **9** (2021).

453 18. L. Coutte *et al.*, Combined RNAseq and ChIPseq Analyses of the BvgA Virulence Regulator of
454 Bordetella pertussis. *mSystems* **5** (2020).

455 19. A. T. Tveit *et al.*, Widespread soil bacterium that oxidizes atmospheric methane. *Proc Natl Acad Sci*
456 *U S A* **116**, 8515-8524 (2019).

457 20. N. Hirth *et al.*, Full Copper Resistance in Cupriavidus metallidurans Requires the Interplay of Many
458 Resistance Systems. *Appl Environ Microbiol* **89**, e0056723 (2023).

459 21. E. Severi, G. H. Thomas, Antibiotic export: transporters involved in the final step of natural
460 product production. *Microbiology (Reading)* **165**, 805-818 (2019).

461 22. F. H. Müller *et al.*, Coupling of the pathway of sulphur oxidation to dioxygen reduction:
462 characterization of a novel membrane-bound thiosulphate:quinone oxidoreductase. *Mol Microbiol*
463 **53**, 1147-1160 (2004).

464 23. S. Nambi *et al.*, The Oxidative Stress Network of Mycobacterium tuberculosis Reveals Coordination
465 between Radical Detoxification Systems. *Cell Host Microbe* **17**, 829-837 (2015).

466 24. V. Waschulin *et al.*, Biosynthetic potential of uncultured Antarctic soil bacteria revealed through
467 long-read metagenomic sequencing. *ISME J* **16**, 101-111 (2022).

468 25. C. E. Alvarez-Martinez, R. L. Baldini, S. L. Gomes, A Caulobacter crescentus extracytoplasmic
469 function sigma factor mediating the response to oxidative stress in stationary phase. *J Bacteriol* **188**,
470 1835-1846 (2006).

471 26. X. Hao *et al.*, A role for copper in protozoan grazing - two billion years selecting for bacterial copper
472 resistance. *Mol Microbiol* **102**, 628-641 (2016).

473 27. G. Prunier *et al.*, Fast alignment of mass spectra in large proteomics datasets, capturing
474 dissimilarities arising from multiple complex modifications of peptides. *BMC Bioinformatics* **24**, 421
475 (2023).

476 28. J. K. Lewis *et al.*, New Role for Radical SAM Enzymes in the Biosynthesis of Thio(seleno)oxazole
477 RiPP Natural Products. *Biochemistry* **60**, 3347-3361 (2021).

478 29. K. Wüthrich, *NMR of proteins and nucleic acids* (Wiley, New York, 1986).

479 30. D. S. Wishart, C. G. Bigam, A. Holm, R. S. Hodges, B. D. Sykes, 1H, 13C and 15N random coil
480 NMR chemical shifts of the common amino acids. I. Investigations of nearest-neighbor effects. *J*
481 *Biomol NMR* **5**, 67-81 (1995).

482 31. M. Sattler, Heteronuclear multidimensional NMR experiments for the structure determination of
483 proteins in solution employing pulsed field gradients. *Progr. Nucl. Magn. Reson. Spectr.* **34**, 93-158
484 (1999).

485 32. T. Yamazaki, W. Lee, C. H. Arrowsmith, D. R. Muhandiram, L. E. Kay, A Suite of Triple Resonance
486 NMR Experiments for the Backbone Assignment of 15N, 13C, 2H Labeled Proteins with High
487 Sensitivity. *J. Am. Chem. Soc.* **116**, 11655-11666 (1994).

488 33. K. E. Fiore *et al.*, Structural impact of thioamide incorporation into a beta-hairpin. *RSC Chem Biol*
489 **3**, 582-591 (2022).

490 34. V. Wray, "Progress in NMR Spectroscopy". (1979), vol. 13, pp. 177-256.

491 35. G. E. Kenney, A. C. Rosenzweig, Chalkophores. *Annu Rev Biochem* **87**, 645-676 (2018).

492 36. B. Bennett, J. M. Kowalski, EPR Methods for Biological Cu(II): L-Band CW and NARS. *Methods*
493 *Enzymol* **563**, 341-361 (2015).

494 37. F. Bonardi *et al.*, Probing the SecYEG translocation pore size with preproteins conjugated with
495 sizable rigid spherical molecules. *Proc Natl Acad Sci U S A* **108**, 7775-7780 (2011).

496 38. K. A. Clark, M. R. Seyedsayamdost, Bioinformatic Atlas of Radical SAM Enzyme-Modified RiPP
497 Natural Products Reveals an Isoleucine-Tryptophan Crosslink. *J Am Chem Soc* **144**, 17876-17888
498 (2022).

499 39. A. A. DiSpirito *et al.*, Methanobactin and the Link between Copper and Bacterial Methane
500 Oxidation. *Microbiol Mol Biol Rev* **80**, 387-409 (2016).

501 40. G. E. Kenney, A. C. Rosenzweig, Methanobactins: Maintaining copper homeostasis in
502 methanotrophs and beyond. *J Biol Chem* **293**, 4606-4615 (2018).

503 41. Y. Li *et al.*, Discovery and biosynthesis of tricyclic copper-binding ribosomal peptides containing
504 histidine-to-butyrine crosslinks. *Nat Commun* **14**, 2944 (2023).

505 42. J. D. Semrau, A. A. DiSpirito, P. K. Obulisamy, C. S. Kang-Yun, Methanobactin from
506 methanotrophs: genetics, structure, function and potential applications. *FEMS Microbiol Lett* **367**,
507 fnaa045 (2020).

508 43. H. Büttner, J. Hörl, J. Krabbe, C. Hertweck, Discovery and biosynthesis of anthrochelin, a growth-
509 promoting metallophore of the human pathogen *Luteibacter anthropi*. *ChemBioChem* **24**, e202300322
510 (2023).

511 44. E. I. Koh, A. E. Robinson, N. Bandara, B. E. Rogers, J. P. Henderson, Copper import in
512 Escherichia coli by the yersiniabactin metallophore system. *Nat Chem Biol* **13**, 1016-1021 (2017).

513 45. B. M. Staehlin, J. G. Gibbons, A. Rokas, T. V. O'Halloran, J. C. Slot, Evolution of a Heavy Metal
514 Homeostasis/Resistance Island Reflects Increasing Copper Stress in Enterobacteria. *Genome Biol*
515 *Evol* **8**, 811-826 (2016).

516 46. Z. Yu, L. Gunn, P. Wall, S. Fanning, Antimicrobial resistance and its association with tolerance to
517 heavy metals in agriculture production. *Food Microbiol* **64**, 23-32 (2017).

518 47. C. Baker-Austin, M. S. Wright, R. Stepanauskas, J. V. McArthur, Co-selection of antibiotic and
519 metal resistance. *Trends Microbiol* **14**, 176-182 (2006).

520 48. K. S. Chaturvedi, J. P. Henderson, Pathogenic adaptations to host-derived antibacterial copper.
521 *Front Cell Infect Microbiol* **4**, 3 (2014).

522 49. J. R. Sheldon, E. P. Skaar, Metals as phagocyte antimicrobial effectors. *Curr Opin Immunol* **60**, 1-9
523 (2019).

524 50. L. Novoa-Aponte, C. Xu, F. C. Soncini, J. M. Arguello, The Two-Component System CopRS
525 Maintains Subfemtomolar Levels of Free Copper in the Periplasm of Pseudomonas aeruginosa
526 Using a Phosphatase-Based Mechanism. *mSphere* **5** (2020).

527

528

529

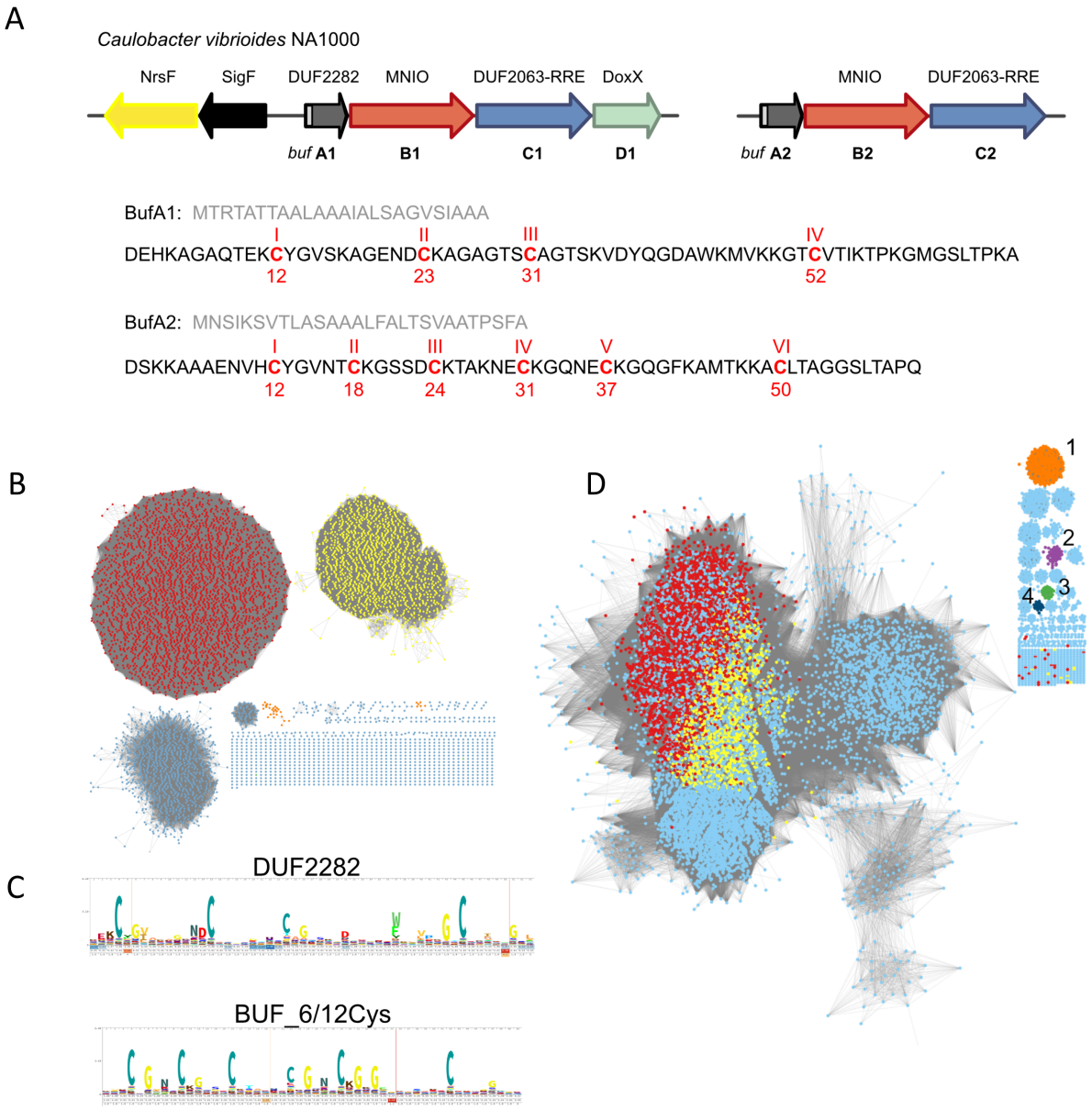

Figure 1. *In silico* analyses of the bufferin family. A. Gene composition of the *buf1* and *buf2* BGCs and sequences of BufA1 and BufA2 with the Cys residues labeled (numbering according to the core peptides). The signal peptide and core peptide sequences are in pale and dark grey, respectively. In the vicinity of *buf1ABCD* are genes coding for SigF and the anti-sigma factor NrsF that regulate *buf1* and *buf2* expression. **B**. SSN analysis of bufferin-like precursors genetically associated with MNIOs. DUF2282 and BUF_6/12Cys proteins, including BufA1 and BufA2 of *C. vibrioides*, belong to the largest two clusters (red and yellow dots), respectively. Small clusters in orange contain the RiPPs of *Chryseobacterium* (7) that are predicted to harbor signal peptides. **C**. Weblogos for the DUF2282 and BUF_6/12Cys bufferins. **D**. SSN analysis of MNIOs (at 80% identity). MNIOs genetically associated with DUF2282 and BUF_6/12Cys proteins, including BufB1 and BufB2 of *C. vibrioides*, are in red and yellow, respectively. MNIOs associated with PTMS on methanobactins, *Chryseobacterium* RiPPs, TglA-type pearlins and aminopyruvatides are found in small clusters numbered 1 to 4.

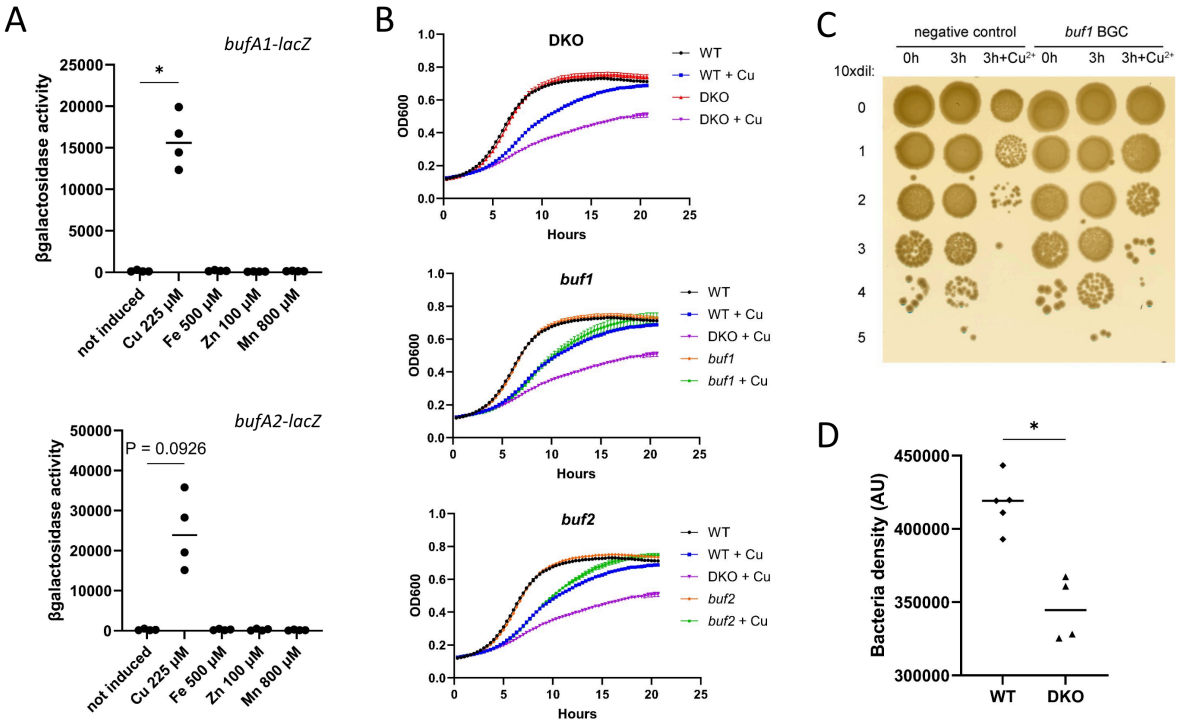

Figure 2. Regulation and function of the bufferins. **A**. Reporter assays with *bufA1-lacZ* and *bufA2-lacZ* transcriptional fusions. Bacteria were grown for 16 h with the indicated concentrations of $CuSO_4$, $FeSO_4$, $ZnSO_4$ or $MnCl_2$. Non-parametric, one-way analysis of variance Kruskal-Wallis (two-sided) tests followed by a Dunn's multiple-comparison tests were used to analyze the differences between treated cultures and the control (n=4; * in the upper left graph indicates p=0.047). **B**. Effect of copper on bacterial growth. The Cv_{DKO}, $Cv_{buf1ABCD}$ (*buf1)* and $Cv_{buf2ABC}$ (*buf2*) strains were grown without or with 225 µM $CuSO_4$. **C**. Gain-of-function assay. Expression of *buf1* in *E. coli* BL21(pCA24-buf1A^{str}BCD) was induced by IPTG, and the bacteria were challenged with 0.3 mM $CuSO_4$ for three hours before serial dilutions. BL21(pCA24-psmCA) expressing a non-relevant RiPP BGC was used as a control. **D**. Assay of bacterial lysis by *D. discoidum*. Bacterial densities of the lysis plaques were determined using ImageJ analyses. A non-parametric Mann-Whitney test (two-sided) was used to analyze the differences between the Cv_{WT} strain (n=5) and the Cv_{DKO} strain (n=4; * indicates p = 0.0159). The medians are shown.

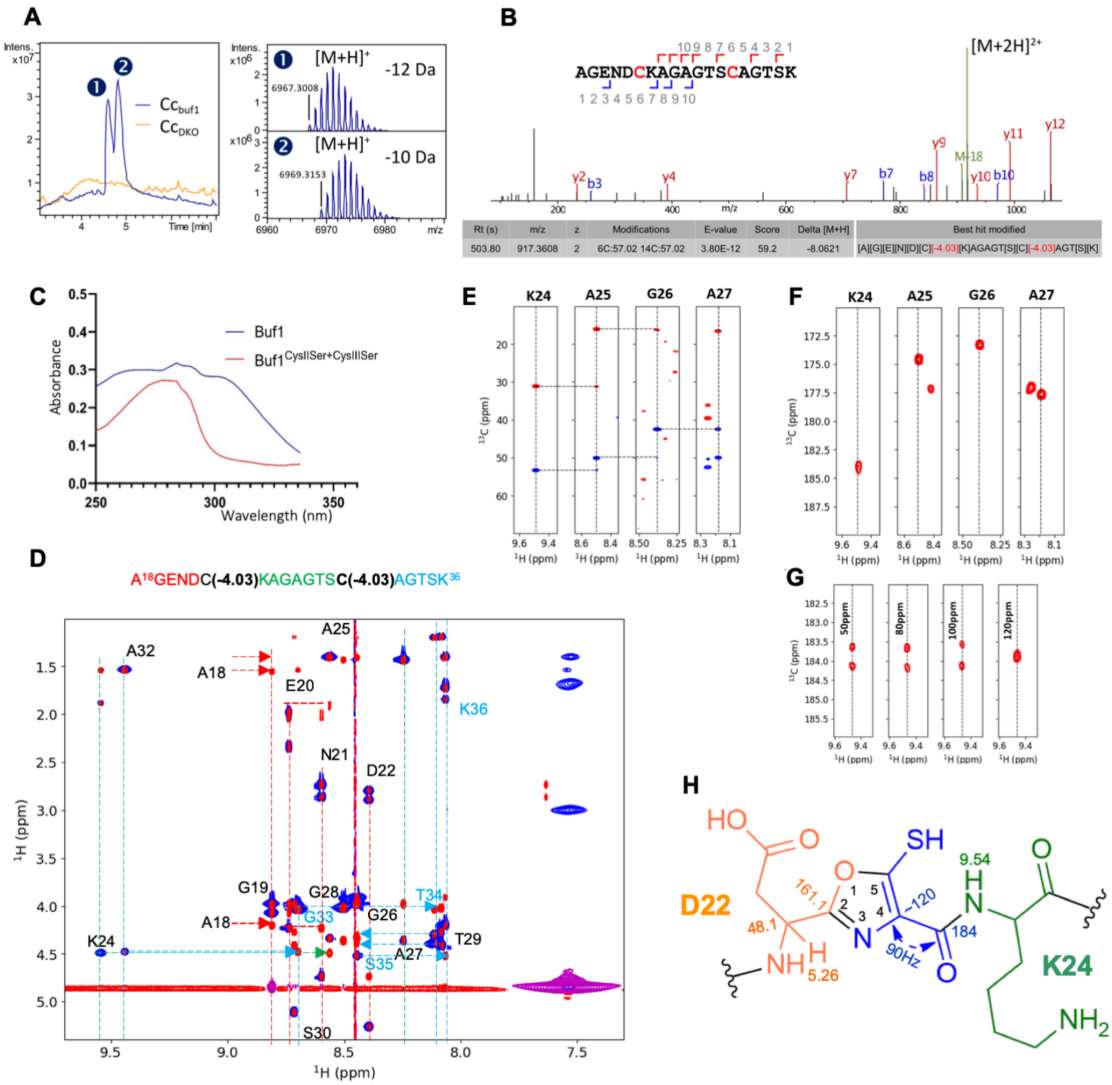

Figure 3. Post-translational modifications of bufferin 1. **A.** Top-down LC-MS analyses of cell extracts of Cv_{buf1}(pSigF) compared with Cv_{DKO}(pSigF). Left panel: total ion chromatograms, right panels: deconvoluted mass spectra of the compounds detected for Cv_{buf1}(pSigF). Their Mw correspond to the core peptide (*i.e.*, without signal peptide; calculated monoisotopic Mw=6978.35 Da), with mass shifts of -10 Da ($[M+H]^+$ at *m/z* 6969.32) and -12 Da ($[M+H]^+$ at *m/z* 6967.30). **B.** Bottom-up analysis of Buf1. MS/MS spectrum of the central tryptic peptide ($[M+2H]^{2+}$ at *m/z* 917.36). The two Cys residues carry carbamidomethyl groups resulting from alkylation with iodoacetamide (+ 57.02 Da), together with -4.03 Da mass shifts. **C.** UV/vis spectra of affinity-purified Buf1 and the Cys^{II}Ser+Cys^{III}Ser mutant. **D.** NMR ROESY/TOCSY experiments to assign the resonances of the 19-mer peptide. **E**. HNCACB experiment on the uniformly ^{13}C, ^{15}N-labeled peptide: sequential walk for the sequence following Cys^{II}. **F**. The HNCO planes at the ^{15}N frequency of the indicated residues show classical ~175-ppm values for all carbonyl resonances, except for that downstream of a modified Cys, whose carbonyl carbon resonates at 184 ppm. **G**. HNCO planes through the resonance of Lys24 that follows Cys^{II} while modifying the offset of the ^{13}C decoupling pulse during the C=O evolution period. Only when centered at 120 ppm is the 90-Hz carbon-carbon coupling refocused. **H.** Measured NMR parameters and proposed structure for the Buf1 post-translational modifications (shown for Cys^{II}).

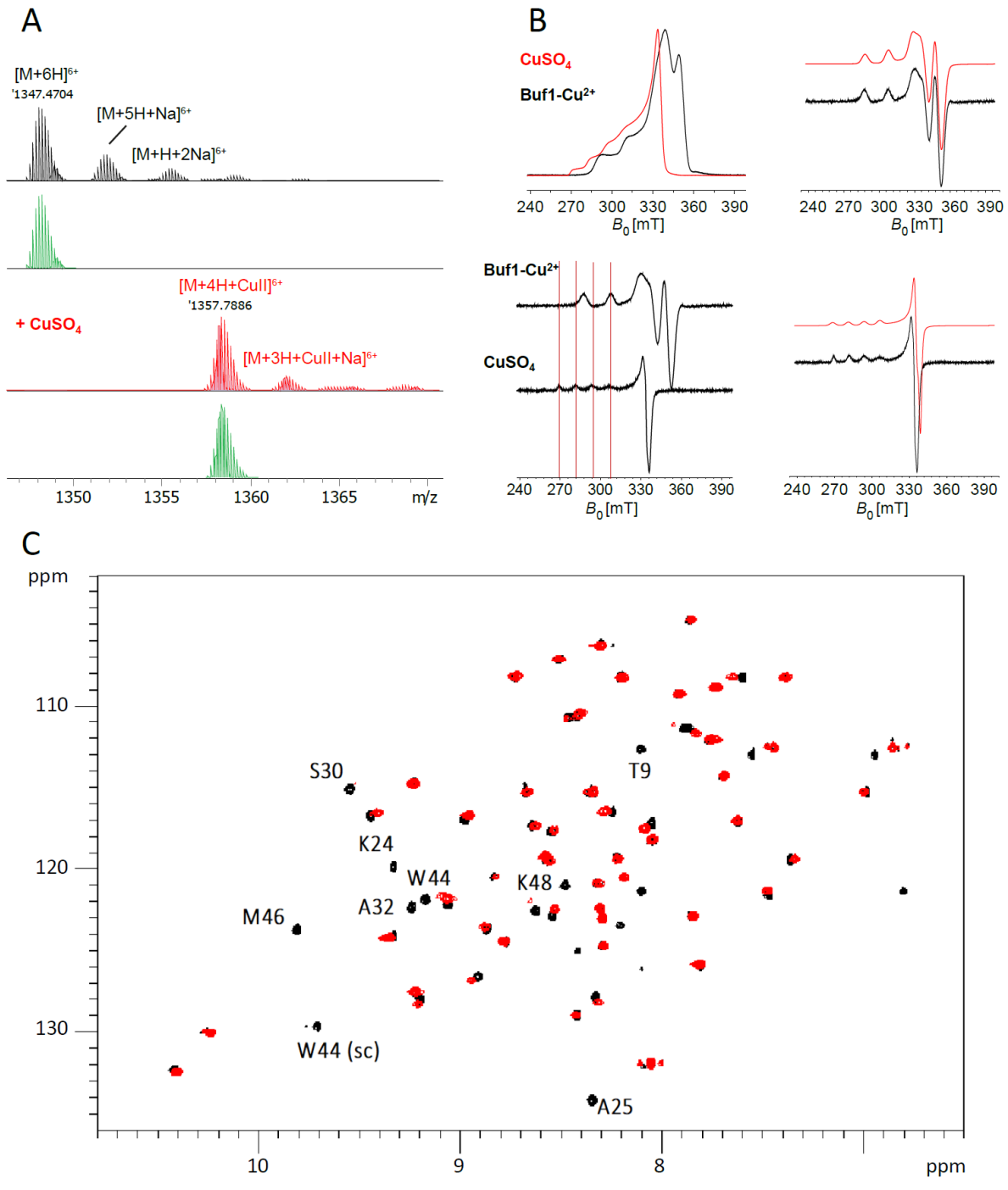

Figure 4. Analyses of the bufferin 1-copper complex formed *in vivo*. A. Native MS analysis of the purified complex: isotopic patterns of the major charge state (6+) species. The spectra in black and red show Buf1 from a non-supplemented culture and from cultures supplemented with $CuSO_4$, respectively. The calculated isotopic patterns for $[M+6H]^{6+}$ and $[M+4H+CuII]^{6+}$ species are shown in green. **B.** Evidence for Cu^{2+} binding to Buf1 by EPR spectroscopy. Spectra of Echo-Detected Field-Swept of $CuSO_4$ (red) and of the Buf1-Cu^{2+} complex (black) are shown with the pseudo-modulation of the spectra underneath. The right panels show the Easyspin fits (red) and the experimental spectra (black) for the Buf1-Cu^{2+} complex (top) and for $CuSO_4$ (bottom). **C.** Superposition of the ^{1}H, ^{15}N HSQC spectra of apo Buf1 (black) and the Buf1-Cu^{2+} complex (red). sc= side chain.

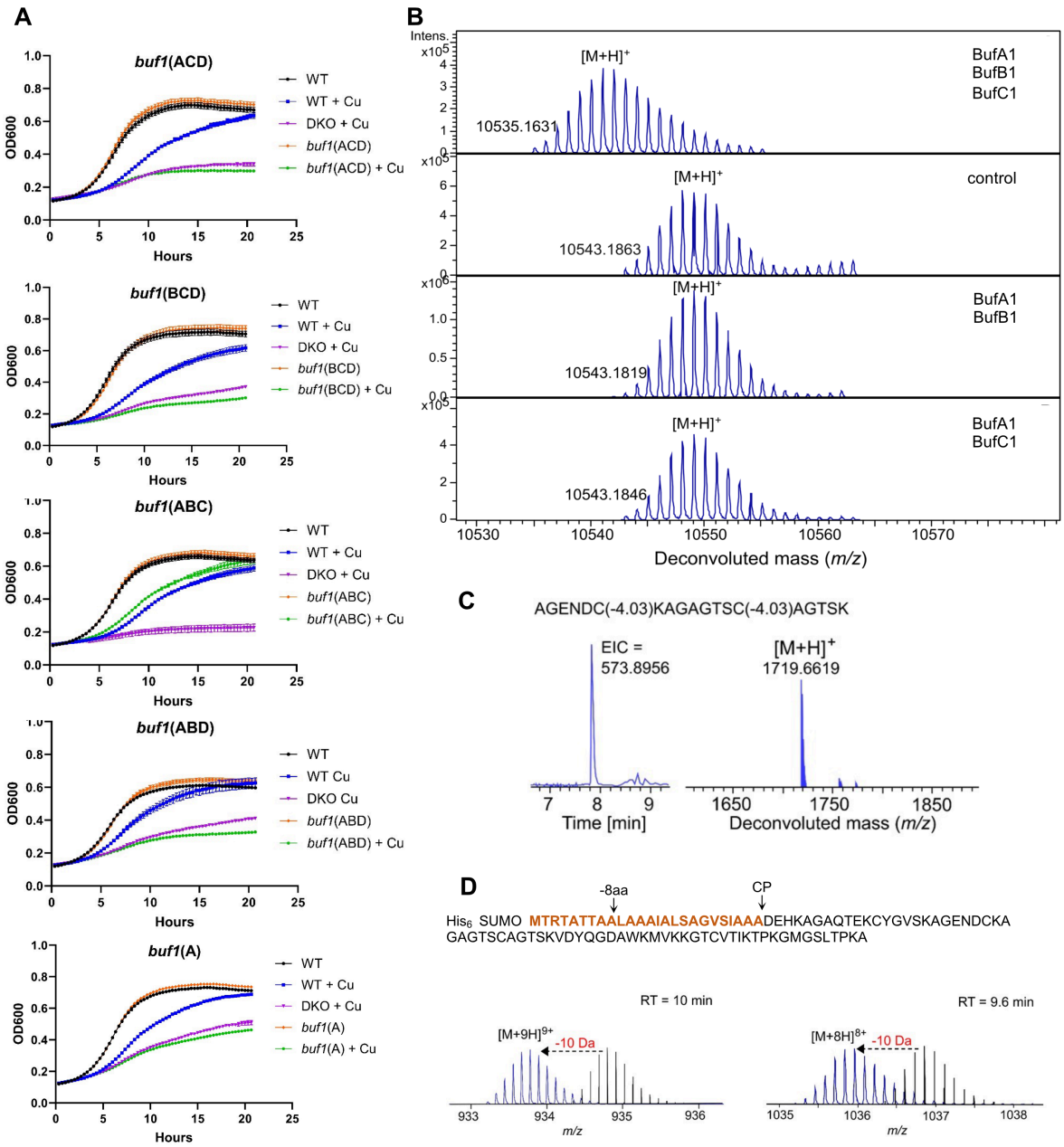

Figure 5. Biosynthesis of bufferin 1. A. Effect of Cu on the growth of *C. vibrioides* strains expressing the indicated genes. **B.** *In vitro* reconstitution of Buf1 biosynthesis. The deconvoluted mass spectra for the products of the *in vitro* reactions are shown, with the added proteins indicated in the corresponding panels. Heat-denatured BufB1 and BufC1 were used for the control reaction. **C.** LC-MS analysis of the 19-residue peptide of *in vitro* modified SUMO-Buf1. The extracted ion chromatogram (EIC) of $[M+3H]^{3+}$ (at *m/z* 573.8945) and the deconvoluted mass are shown. **D**. Role of the signal peptide for the PTMs. A schematic representation of BufA1 variants with signal peptide truncations is shown on top. LC-MS analyses of modified BufA1(-8 aa) (left) and modified BufA1(CP) (right): the MS spectra of the most abundant charge states $[M+9H]^{9+}$ and $[M+8H]^{8+}$, corresponding to deconvoluted monoisotopic masses $[M+H]^{+}$ of 8391.1281 and 8277.9398 (blue), respectively, are compared to the theoretical spectra of the unmodified peptides (black).